Ab-initio transport study of Source-to-Channel Resistance in Metal-MoS_2 Top Contacts including Image Force Barrier Lowering in a Heterogeneous Dielectric Environment

Alessandro Pilotto, Daniel Lizzit, Marco Pala, David Esseni
DPIA, University of Udine, Via delle Scienze 206, 33100 Udine, Italy.
e-mail: alessandro.pilotto@uniud.it, daniel.lizzit@uniud.it, marco.pala@uniud.it, david.esseni@uniud.it

***Abstract*—We present an *ab-inito* transport study, based on the Density Functional Theory (DFT) and the non-equilibrium Green's Functions (NEGF) formalism, to assess the effect of the Image Force Barrier Lowering (IFBL) on the source-to-channel resistance (R_C) in metal-MoS_2 top contacts. To compute the IFBL potential profile, our model relies on the numerical solution of the 3D Poisson equation for the point charge in a heterogeneous dielectric environment.**

By considering Al–MoS_2 and Bi–MoS_2 van-der-Waals heterojunctions, representative of a Schottky and an Ohmic contact respectively, we show that, while for Schottky contacts the inclusion of the IFBL has a vast impact on the source-to-channel resistance, in quasi-Ohmic contacts the influence of the IFBL on the R_C becomes negligible, especially at large inversion densities.

***Index Terms*—*ab-initio*, NEGF, IFBL, Contact Resistance**

I. Introduction

Among two-dimensional (2D) semiconducting materials, monolayer Transition Metals Dichalcogenides (TMDs) have drawn attention as viable candidates for channel materials in nanoelectronic devices. One of the biggest challenges in the integration of TMDs in future technology nodes is the realization of metal-TMD interfaces with low contact resistance. In fact, metal-induced-gap-states can induce Fermi level pinning at metal-TMD interfaces, which results in large Schottky barrier heights (SBHs) and deteriorates the contact resistance. Given such a Schottky nature, the contact resistance R_C depends not only on the material properties of the metal-MoS_2 heterojunction, but also on the gate-bias dependent band profile close to the contact and in the channel region.

In recent years, the effect of the SBH on R_C has been extensively studied by means of experiments [1], and numerical simulations (see for example [2] and references therein). DFT calculations, however, do not include the effects of IFBL, unless performed at the GW level [3]. Analytical expressions to derive the IFBL potential for a large variety of contact geometries have been derived in the case of homogeneous dielectrics [4], and then used to compute R_C for metal-MoS_2 contacts with the quantum boundary transmitting method [2], [4]. In this paper, numerical solutions of the 3D Poisson's equation are used to describe the IFBL potential for a metal–monolayer MoS_2 vertical heterojunction (VHJ) accounting for the heterogeneous dielectric environment. The IFBL potential is then added to the potential obtained from the self–consistent solution of the non-equilibrium Green's functions (NEGF) and Poisson's equations [5], to calculate the quasi-equilibrium R_C of the device shown in Fig. 1. Our approach employs an *ab-initio* description of the metal-MoS_2 heterojunction with Hamiltonians obtained from DFT calculations [6].

Funded by the European Union (Horizon Europe, AttoSwitch, GA no. 101135571). Views and opinions expressed are however those of the authors only and do not necessarily reflect those of the European Union or the European Commission. Neither the European Union nor the granting authority can be held responsible for them..

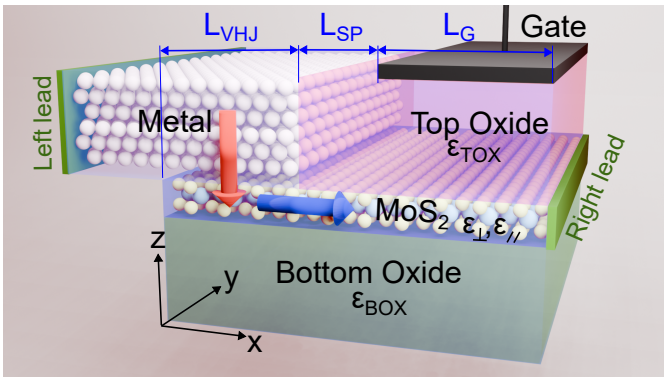

case A	no IFBL
case B	homogeneous permittivity, $\varepsilon_{diel}=3.9\varepsilon_0$
case C	heterogeneous permittivity

Fig. 1. Sketch of the simulated structure used to extract R_C. The top metal-MoS_2 contact has a length L_{VHJ}=15 nm. An L_{SP}=5 nm long spacer separates the gate (L_G=15 nm) from the VHJ. The relative permittivities are ε_{TOX}=22, ε_{BOX}=3.9 for the dielectrics, and $\varepsilon_\perp$=6.1, $\varepsilon_{||}$=15.4 for MoS_2. Left and right semi-infinite leads are shown in green, and in this work their potential is set to simulate quasi-equilibrium conditions. Arrows indicate the contributions to R_C related to the presence of a VHJ (red arrow), and of possible potential barriers towards the channel region (blue arrow). Case A, B, C in the table are the three case studies addressed in this work.

The results of this work show that: *i)* when the SBH at the VHJ is large compared to the thermal energy k_BT, the inclusion of the IFBL has a vast impact on R_C; *ii)* in quasi-ohmic contacts, where SBH is smaller than k_BT (or even negative), the influence of the IFBL on the R_C becomes negligible, especially at large inversion densities; *iii)* the

heterogeneous dielectric environment has a sizeable impact on the IFBL and consequently on R_C.

The paper proceeds as follows: Section II describes the methodology used to numerically compute the Image Force Barrier Lowering potential for metal-TMD top contacts in a heterogeneous dielectric environment. Section III gives some details on the *ab-initio* NEGF simulations used throughout this work for the calculation of the source-to-channel resistance. Finally, Section IV reports the main results while final remarks are given in Section V.

II. IFBL Potential

The simulation setup consists of a metal-MoS_2 VHJ and a MoS_2 region that extends outside the VHJ sandwiched between a top and a bottom oxide as shown in Fig. 1. By following [4], the image-force potential energy $U_{\text{IFBL}}(\mathbf{r}_0)$ is defined and calculated as

$$U_{\text{IFBL}}(\mathbf{r}_0) = -\frac{1}{2} e V_{\text{I}}(\mathbf{r}_0), \tag{1}$$

where e is the positive electron charge and $\mathbf{r}_0$ is the position of the point charge. The $V_{\text{I}}(\mathbf{r})$ is defined as

$$V_{\text{I}}(\mathbf{r}) = V(\mathbf{r}) - V_{\text{C}}(\mathbf{r}). \tag{2}$$

namely it is the difference between the electrostatic potentials generated by a point charge in $\mathbf{r}_0$ and calculated by either *accounting for*, $V(\mathbf{r})$, or *neglecting*, $V_{\text{C}}(\mathbf{r})$, the metal contact region.

Both $V(\mathbf{r})$ and $V_{\text{C}}(\mathbf{r})$ were obtained by numerically solving the 3D Poisson's equation in (3)

$$\nabla \cdot (\varepsilon(\mathbf{r}) \nabla V(\mathbf{r})) = +e\,\delta(\mathbf{r} - \mathbf{r}_0). \tag{3}$$

Figure 1 defines the three scenarios compared throughout the paper, namely: case A (no IFBL), case B (the IFBL potential profile is computed by considering a homogeneous dielectric permittivity $\varepsilon_{\text{diel}}$=3.9$\epsilon_0$), case C (the computation of the IFBL potential profile considers the heterogeneous dielectric environment of the contact). In plots (a) and (b) of Fig. 2, we show the contour plot of the U_{IFBL}, numerically calculated as explained above and for cases B and C. As a validation of our IFBL model, in Fig. 2(c) we show the good agreement between the U_{IFBL} along the z–direction calculated in this work (case B) with the analytical expression in [4].

III. *Ab-initio* NEGF Simulations including IFBL

We start from DFT calculations with Quantum ESPRESSO [6] of the VHJ and of the isolated metal and MoS_2 to extract the plane-wave Hamiltonians. The details of the calculations for the systems under study are given in [7], [8]. Then, by using the Green Tea simulator [5], self-consistent simulations of the device in Fig. 1 are used to determine, for different gate biases, the band profile and the inversion charge (N_{inv}) in the MoS_2 region outside the contact. Finally, U_{IFBL} is added to the 3D self-consistent potential and, by using Eq. (4), we calculate the spectrum $G_{k_y}(E)$ of the ballistic conductance between the two leads shown in Fig. 1 from the electronic transmission $T_{k_y}(E)$, whereby k_y is the transverse wavevector. Then, the resistance R_C is given by Eq. (5).

$$G_{k_y}(E) = \frac{n_{sp} q^2}{h} T_{k_y}(E) \left(-\frac{df_0(E)}{dE} \right) \tag{4}$$

$$\frac{1}{R_C} = \frac{1}{2\pi} \int_{k_y} \left[\int_{-\infty}^{\infty} G_{k_y}(E) dE \right] dk_y \tag{5}$$

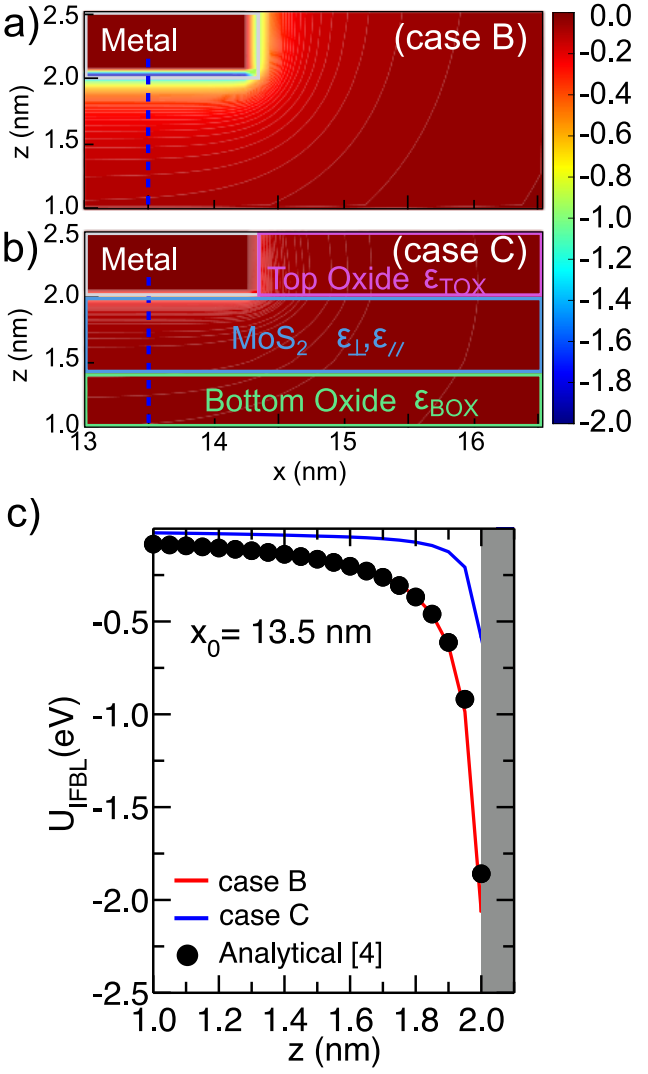

Fig. 2. (a) Contour plot of the numerically calculated image-force potential energy (U_{IFBL}) when a uniform dielectric constant $\varepsilon = 3.9\varepsilon_0$ is considered (case B) for the top oxide, monolayer MoS_2, and the bottom oxide (picture consistent with [2], [4]). (b) same as (a) but with the heterogeneous dielectric environment shown in Fig. 1 (case C). In both cases the mesh for numerical calculations features $\Delta x = 0.1$ nm, $\Delta z = 0.05$ nm, $\Delta y = 0.1$ nm. (c) Comparison between the U_{IFBL} versus z along the dotted blue line drawn in (a)-(b), obtained either with the analytical expression of [4], or with the numerical calculations of this work. The shaded area represents the metal region.

IV. Results

We here focus on the estimation of R_C by simulating the three scenarios reported in Fig. 1 for two different metal–MoS_2 VHJs, namely Al–MoS_2 and Bi–MoS_2 (see Fig. 3), respectively representative of a Schottky (SBH≈200 meV) and an Ohmic contact (SBH≈−10 meV) [8]. For the Al-MoS_2 contact, the orthorhombic supercell is obtained by matching a 2×2 (111) surface of a six-layer Al crystal to a $\sqrt{3} \times \sqrt{3}$ monolayer MoS_2 supercell. On the other hand, for

simulations of Bi-MoS_2 contact, a 2×2 supercell of three Bi (0001) layers has been matched to a $\sqrt{7} \times \sqrt{7}$ MoS_2 cell. In both cases, all the strain has been put on the metal, leaving the monolayer MoS_2 unstrained.

Figures 4(a)-(b) show the spectra of the conductance, obtained by summing the contributions $G_{k_y}(E)$ for all the transverse wavevectors included in our calculations, for the Al-MoS_2 VHJ together with the MoS_2 conduction band minimum (CBM) for case A and case B, computed from a self-consistent simulation at a gate bias inducing $N_{\text{inv}} \approx 12 \cdot 10^{12}$ cm^{-2} in the gated region. The inclusion of the IFBL reduces the SBH within the VHJ and along the transport direction, thus increasing the transmission coefficient, as it is clearly displayed in Fig. 5.

Figures 6(a)-(b) show the CBM profiles without (case A) and with (case C) the inclusion of the IFBL accounting for a heterogeneous dielectric environment for the two simulated VHJs. The corresponding R_C values are shown in Figs.6(c)-(d), where the results for a homogeneous dielectric environment (case B) are also shown. The homogeneous low permittivity of $\varepsilon_{\text{diel}}$=3.9$\varepsilon_0$ (case B) overestimates the magnitude of the U_{IFBL} (see Fig. 2) thus leading to a much lower R_C compared to a more realistic dielectric environment (case C).

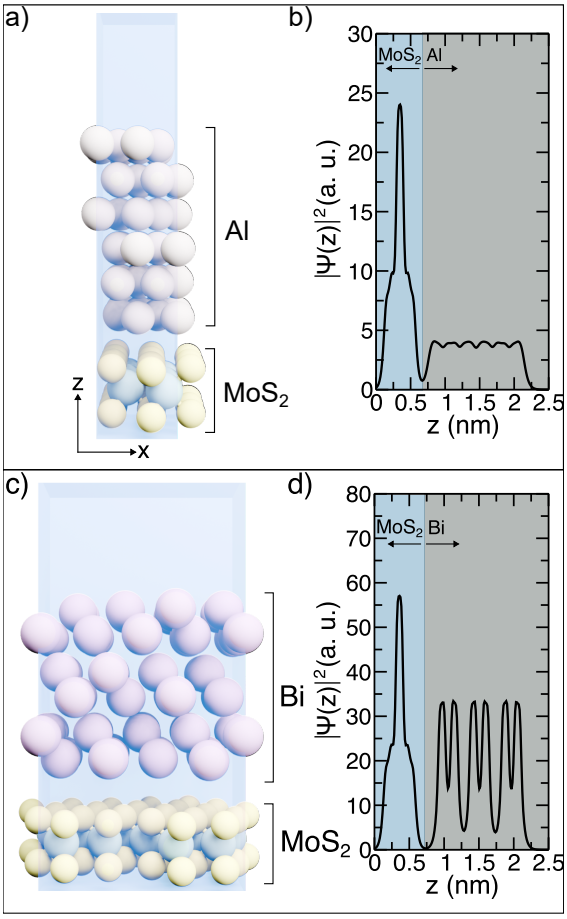

Fig. 3. (a)(c) Side view of the orthorhombic unit cells of the Al-MoS_2 VHJ (a) and the Bi-MoS_2 VHJ (b) used in the *ab-initio* NEGF simulations (detalis in [7], [8]). (b)(d) Average along the x–y plane of the squared modulus of the wavefunctions Ψ in the unit cells in (a) and (c), respectively. The minimum of $|\Psi(z)|^2$ in the region between the MoS_2 and the metal was used to determine the thickness of MoS_2 in our U_{IFBL} calculations.

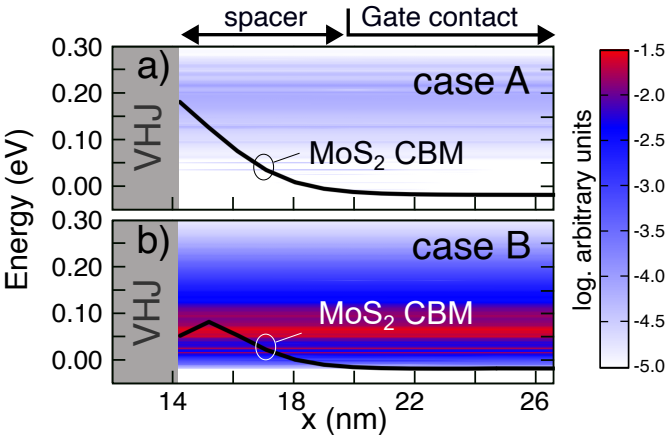

Fig. 4. Spectra of the quasi-equilibrium conductance along the transport direction without IFBL (a), and with IFBL using a homogeneous permittivity $\varepsilon_{\text{diel}}$=3.9$\varepsilon_0$ (b) for the Al-MoS_2 VHJ. The gate bias sets the CBM of MoS_2 in the channel about 17 meV below E_F, corresponding to $N_{\text{inv}} \approx 12 \cdot 10^{12}$ cm^{-2}. The energies are relative to the Fermi level, which is set to zero.

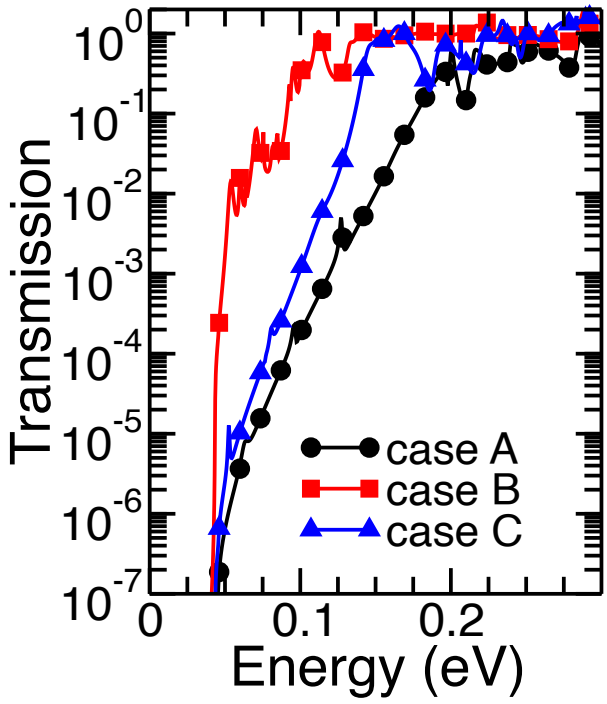

Fig. 5. Transmission coefficient for one transverse k_y=0 without IFBL (case A), with IFBL using the dielectric constants shown in Fig.1 (case C), and using a homogeneous $\varepsilon_{\text{diel}}$=3.9$\varepsilon_0$ (case B) as in [4]. The results are consistent with those in Fig.4.

For the Bi-MoS_2 VHJ, while the inclusion of IFBL reduces the height of the potential barrier along the transport direction in the spacer region, its overall effect on R_C is practically negligible (see Fig. 6(d)), particularly for N_{inv} values such that the peak of the potential energy barrier is very close to the Fermi level. Finally, we notice that even for the maximum considered N_{inv} (i.e. $12 \cdot 10^{12}$ cm^{-2}), the R_C calculated in this paper is roughly twice as large the corresponding result in [7], [8] ($R_C \approx 808$ $\Omega \cdot \mu$m versus $R_C \approx 410$ $\Omega \cdot \mu$m). We verified that this is because, in this paper, the potential energy bump in the spacer region (see Fig. 6(b)), resulting from self-consistent calculations, increases R_C beyond our previous calculations assuming simply a flat band profile outside the VHJ [7], [8].

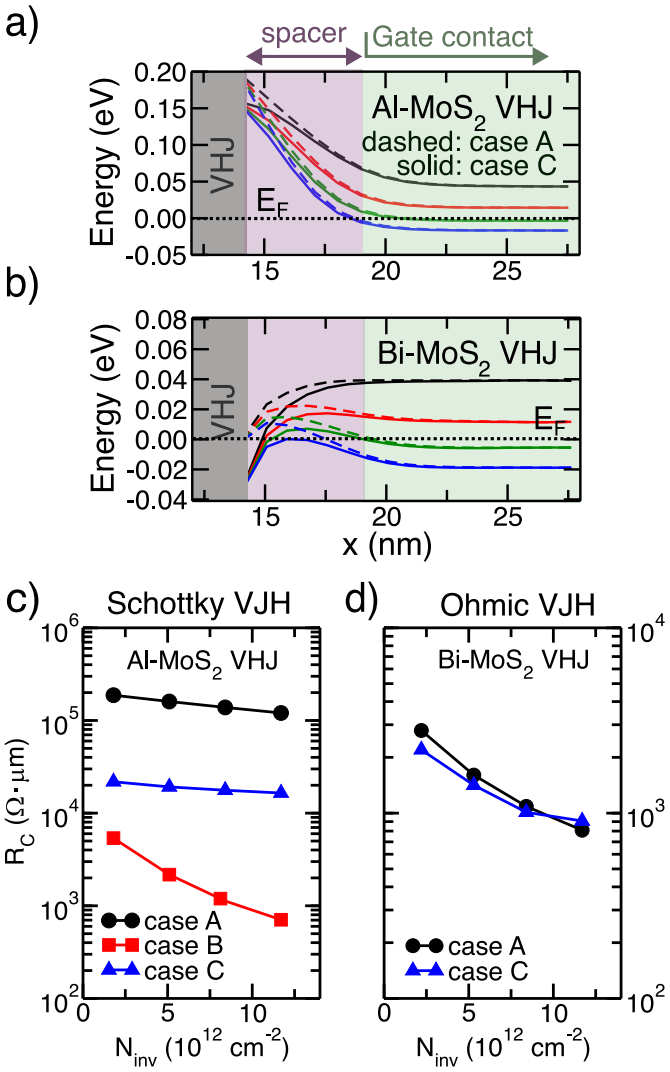

Fig. 6. Conduction band minimum along the transport direction calculated from self-consistent NEGF simulations for the Al-MoS_2 (a) and Bi-MoS_2 (b) VHJs. Results are displayed for different gate biases, setting the electron charge in the gated region to $2\cdot10^{12}, 5\cdot10^{12}, 8\cdot10^{12}$, and $12\cdot10^{12}$ cm^{-2}. The inclusion of the IFBL accounting for a non homogeneous dielectric environment (case C) is shown in solid lines. (c)(d) R_C values obtained for different N_{inv} values and for the three different treatments of the IFBL summarized in Fig.1.

V. Conclusions

We have successfully included the Image Force Barrier Lowering effect accounting for a heterogenous dielectric environment in *ab-initio* quantum transport simulations of metal-TMD top-contacts based on vertical van der Waals heterojunctions.

Our calculations of the source-to-channel resistance (R_C) in top-gated structures show that the IFBL has a significant impact on the value of R_C only in those systems where the Schottky barrier height is large compared to k_BT. On the other hand, in those systems that exhibit a quasi-ohmic behavior, the influence of the IFBL on the R_C becomes negligible, in particular for gate biases that correspond to large inversion densities ($\approx 10^{13}$ cm^{-2}).

References

[1] D. Akinwande, C. Biswas, and D. Jena, "The quantum limits of contact resistance and ballistic transport in 2D transistors," *Nature Electronics*, vol. 8, no. 2, pp. 96–98, Feb 2025. doi: 10.1038/s41928-024-01335-5

[2] P. Baikadi, W. Vandenberghe, P. Reyntjens, R. Kim, and M. Van de Put, "Quantum transport study of transition-metal dichalcogenide top-contacted geometries investigating the impact of nonuniform doping, dielectric environment, and image-force barrier lowering," *Phys. Rev. Appl.*, vol. 22, p. 064058, Dec 2024. doi: 10.1103/PhysRevApplied.22.064058

[3] C. Li, M. Bescond, and M. Lannoo, "GW investigation of interface-induced correlation effects on transport properties in realistic nanoscale structures," *Phys. Rev. B*, vol. 80, p. 195318, Nov 2009. doi: 10.1103/PhysRevB.80.195318

[4] S. R. Evans, E. Deylgat, E. Chen, and W. G. Vandenberghe, "Image-force barrier lowering of Schottky barriers in two-dimensional materials as a function of metal contact angle," *Phys. Rev. Appl.*, vol. 20, p. 044003, Oct 2023. doi: 10.1103/PhysRevApplied.20.044003

[5] M. G. Pala, P. Giannozzi, and D. Esseni, "Unit cell restricted Bloch functions basis for first-principle transport models: Theory and application," *Phys. Rev. B*, vol. 102, p. 045410, Jul 2020. doi: 10.1103/PhysRevB.102.045410

[6] P. Giannozzi, O. Andreussi, T. Brumme, O. Bunau, M. B. Nardelli, M. Calandra, R. Car, C. Cavazzoni, D. Ceresoli, M. Cococcioni, N. Colonna, I. Carnimeo, A. D. Corso, S. de Gironcoli, P. Delugas, R. A. DiStasio, A. Ferretti, A. Floris, G. Fratesi, G. Fugallo, R. Gebauer, U. Gerstmann, F. Giustino, T. Gorni, J. Jia, M. Kawamura, H.-Y. Ko, A. Kokalj, E. Küçükbenli, M. Lazzeri, M. Marsili, N. Marzari, F. Mauri, N. L. Nguyen, H.-V. Nguyen, A. O. de-la Roza, L. Paulatto, S. Poncé, D. Rocca, R. Sabatini, B. Santra, M. Schlipf, A. P. Seitsonen, A. Smogunov, I. Timrov, T. Thonhauser, P. Umari, N. Vast, X. Wu, and S. Baroni, "Advanced capabilities for materials modelling with Quantum ESPRESSO," *Journal of Physics: Condensed Matter*, vol. 29, no. 46, p. 465901, oct 2017. doi: 10.1088/1361-648X/aa8f79

[7] D. Lizzit, P. Khakbaz, F. Driussi, M. Pala, and D. Esseni, "Ab-initio transport simulations unveil the Schottky versus Tunneling barrier trade-off in metal-TMD contacts," in *2022 International Electron Devices Meeting (IEDM)*, pp. 28.2.1–28.2.4, 2022. doi: 10.1109/IEDM45625.2022.10019449

[8] ——, "Ohmic Behavior in Metal Contacts to n/p-Type Transition-Metal Dichalcogenides: Schottky versus Tunneling Barrier Trade-off," *ACS Applied Nano Materials*, vol. 6, no. 7, pp. 5737–5746, 2023. doi: 10.1021/acsanm.3c00166